



Research article

Non-uniform fuel distribution and thermo-mechanical analysis of a 1 MW thermal power micronuclear heat pipe reactor

Umair Aziz^{a,*}, Zafar U. Koreshi^b, Hamda Khan^c, Shakil R. Sheikh^a^a Department of Mechatronics Engineering, Air University, Islamabad, Pakistan^b Faculty of Graduate Studies, Air University, Islamabad, Pakistan^c Department of Sciences & Humanities, National University of Computer and Emerging Sciences, Islamabad, Pakistan

ARTICLE INFO

Keywords:

COMSOL
Micronuclear heat pipe reactors
Monte Carlo simulation
Multiphysics
Structural mechanics
Thermo-mechanics

ABSTRACT

One of the goals in improving the design of compact portable micronuclear heat pipe reactors is to enhance their operating life so that they can generate maximum power within safe nuclear, thermal, and mechanical limits and with minimal human intervention. This work carries out an analysis to estimate the effect of non-uniform fuel enrichment and thermo-mechanical performance of a 1 MW thermal power uranium nitride fueled Micro Nuclear Heat Pipe Reactor (MNHPR). For neutronic and thermo-mechanical analyses, the open-source Monte Carlo code OpenMC and the COMSOL Multiphysics codes are used. The neutron flux distribution and subsequent fuel temperature, heat transport, stresses and strains are estimated. The analysis of core power distribution shows an uneven power distribution resulting in hot spots. The maximum fuel centerline temperature of 1353 K at the highest peaking factor 1.22 is within the safety limit. However, the high temperature results in higher thermal stress and subsequent displacement of 119 μm that exceeds the 100 μm fuel-clad gap. Power peaking thus significantly limits the maximum allowed operating power. In this study it is found that non-uniform placement of the fuel reduces power peaking and enhances the overall core performance. It is recommended to consider each fuel ring as a separate zone and gradually change the fuel enrichment in each zone. The non-uniform distribution of the fuel follows the gradual increase of enrichment from ring 1 to ring 5 with max enrichment in ring 5, and then a drop in the enrichment to mitigate any peaking in ring 6 due to its proximity to the reflector. From ring 1 to ring 6 fuel of 60-62-70-70-75-65 percent enrichment is recommended. The proposed fuel strategy mitigates power peaking in the core and enhances the maximum safe operating power level by 15 % from 775 kW to 893 kW without physical design change.

1. Introduction

Recently the world has seen renewed interest in space exploration missions; this renewed interest has led to research in Highly Enriched Uranium (HEU) Micro Nuclear Reactors (MNR) with minimum moving parts [1–4]. These transportable and compact systems also have the potential to replace traditional power systems in decentralized micro-grids to meet the power requirements of off-grid installations.

A conceptual design of a MW thermal power lithium heat pipe based multipurpose micronuclear reactor power source [1]

* Corresponding author.

E-mail addresses: umair.aziz@mail.au.edu.pk, umairaziz@outlook.com (U. Aziz).

minimizes the moving parts while retaining control drums to maintain reactivity in the system and to keep the plant running at desired power. Such a design was based on a uniform core composition which resulted in power peaking [2] causing non-uniform heat removal requirements which could be mitigated by using different fuel enrichments as in nuclear power plants.

Micronuclear reactors in the kilo-power to megawatt range are attractive due to their compact size, mobility, and ability to operate for many years without human intervention. These highly enriched heat-pipe-based MNRs with uniform fuel distribution undergo Radial Power Peaking (RPP) due to irregular burnup of the fuel in different fuel regions. To minimize and mitigate the power peaking in the core, non-uniform fuel distribution and the use of variable conductance heat pipes are amongst possible solutions. The non-uniform fuel distribution uses different enrichment (ϵ) of fuel in different regions or zones of the core.

Evinci [3] is another heat-pipe based design of a small modular reactor from Westinghouse for commercial and off-grid applications. The design focuses on simplicity as the whole system is housed in a steel monolith with housings for fuel, moderator, and heat pipes. Maintaining a flat power distribution in the hexagonal core remains a challenge.

A smaller Kilopower Reactor Using Stirling TechnologY (KRUSTY) [4], designed by NASA for space missions uses heat pipes to remove heat for conversion in Stirling engines. These are in the 1–10 kW_e range and use highly enriched (93 %) fuel which has been experimentally verified [5] for transients and possible excursions.

Micro Nuclear Heat Pipe Reactors (MNHPR) will be subject to detailed coupled analysis covering neutronic, thermal, mechanical and depletion analyses which will be required for regulatory compliance [6]. A vast body of knowledge that exists for nuclear power plants such as Pressurized Water Reactors (PWRs) [7,8] helps considerably in developing reliable models which take into account the metallurgy and mechanical behavior of uranium dioxide [9–12].

Such is the primary motivation for this work also with the differences that MNHPRs are fast reactors and advanced improved accident-tolerant fuels such as uranium nitride are used instead of uranium dioxide in Light Water Reactors. The metallurgy and mechanical behavior of Uranium Nitride (UN) is very different from that of uranium oxides [13,14]. Although UN fuel has a high melting point (3120 K) it starts undergoing decomposition at about 2000K [15] due to low partial pressure of nitrogen. Thus, fuel temperature should be kept within this limit during operation. Further, the thermal conductivity of UN is higher than that of Uranium Dioxide (UO₂) and the former has an advantage that thermal conductivity increases with temperature [13,14].

MNHPRs with thermoelectric generators have also been studied e.g., by Chenglong et al. [16], who have carried out coupled neutronic, thermal hydraulic and conversion analyses of a conceptual heat pipe reactor showing that in case of a single heat pipe failure, the temperature rise is within safety limits, allowing excess heat to be removed by the adjacent heat pipes while the reactor attains a new steady state without compromising the fuel safety.

An elaborate performance analysis for uranium nitride fuel for a lead cooled fast reactor has been carried out by Yuan et al. [15] for thermal loading of 30 kW/m and 45 kW/m power densities as well as for a transient with 60 kW/m. Another similar work by Liu et al. [17], carries out a thermal-hydraulic design analysis of a 500kW_{th} 45 % enriched UN fueled MNR using potassium in a heat pipe. Their analysis was carried out using in-house developed code with modules for the multichannel reactor core neutronics, heat pipe thermal resistance network model, thermal conductivity model, and thermoelectric conversion.

The studies thus far have been carried out while considering the conventional periodic in-core fuel management for large thermal reactors, and uniform distribution of the fuel for MNRs. Detailed investigation into power peaking and fuel placement has remained relatively unexplored. In this study a comprehensive analysis has been carried out to understand the fuel utilization and RPP in the proposed MNR design. This study introduces a unique one-time fuel placement strategy that addresses the power peaking in the reactor core and enhances the overall core performance while diverging from the conventional practice of design change.

In this study, a comprehensive sensitivity analysis for the change in system multiplication due to a change in fuel enrichment ($\delta k_{\text{eff}}/\delta\epsilon$) is carried out for fuel rings in the core using Monte Carlo (MC) simulation code OpenMC [18]. OpenMC is a community developed opensource neutron and photon transport code that was originally developed at Massachusetts Institute of Technology. The code allows to model complex geometries and analyze nuclear reactions, designs, and systems through MC simulations.

MC simulations enable the identification of fuel zones with the highest sensitivity. This analysis thus forms the basis for optimal non-uniform fuel distribution in the core to eliminate the RPP. Additionally, thermal stress from high temperature can compromise the structural integrity of the core, while low temperatures can hinder the performance of sodium heat pipe. Thus, a coupled thermal and solid mechanics analysis has been carried out to determine whether the system can sustain megawatt thermal power operation for years.

Thus, the aim of this paper is twofold: first, to conduct a neutronic search for a one-time fuel placement strategy, differing from the periodic in-core fuel management of conventional high-power thermal reactors; and second, to estimate the thermal stresses and resulting deformations in the fuel. Criticality, self-sustaining chain reaction, is a fundamental aspect in reactor dynamics and while searching for a fuel placement strategy it is pertinent to maintain reactor criticality. A slight change in the fuel placement or enrichment can disturb the minimum critical mass. Thus, a detailed neutronic study is necessary while searching for the fuel placement strategy that mitigates power peaking in such a way that it also ensures that the reactor remains critical i.e., a self-sustaining nuclear chain reaction is maintained. While mitigating the power peaking, it is also important to ensure structural integrity of the fuel and reactor core. Thus, a coupled thermo-mechanical analysis has also been carried out using COMSOL Multiphysics [19] to ensure the structural integrity of the reactor core. COMSOL Multiphysics is a Multiphysics simulation tool that allows to model and simulate physical phenomena across various disciplines including engineering and science. COMSOL Multiphysics' extensive set of toolboxes allows to model complex geometries, add diverse materials and their interactions; it further allows to simulate coupled studies and post process the results.

This work addresses the research gap in MNHPR design practices regarding power distribution in the core by exploring innovative fuel placement strategies. Specifically, the aim is to mitigate radial power peaking, through unique a one-time fuel configuration that

diverges from the conventional practice of periodic in-core fuel management. Additionally, the investigation includes analyzing the thermal stresses and subsequent deformations due to high operating temperatures for better understanding of the reactor performance and to ensure structural integrity of the core.

2. Materials and methods

2.1. Reactor core

The MNR core and radial and axial shields have been modeled using OpenMC code as shown in Fig. 1 (top view) and Fig. 2 (side view), respectively, with the solid matrix core monolith comprising fuel and heat pipes surrounded by the reflectors, the absorber, and the shielding regions.

The reactor core has 90 cylindrical UN fuel rods, and 37 heat pipes to remove thermal energy produced by nuclear fission in the core to the TEG. The hexagonal core is surrounded by six boron carbide (B_4C) tipped control drums embedded within the radial reflector. The objective of this design [1,2] is power conversion from nuclear thermal energy in the core to electrical energy in the Thermo Electric Generator (TEG) without the use of rotating machinery such as pumps and turbines. The main features of the overall core design modeled using OpenMC are listed in Table 1 and Table 2 [1,2].

For neutronics simulations, geometry modeling, and establishing the criticality of the design, the code was run in the eigenvalue mode. For all simulations ENDF/B-VIII.0 cross section library has been used with OpenMC v0.14. 10^5 histories were recorded for 10,000 cycles with 200 inactive cycles. Multiple initial runs were made to observe the source and average multiplication factor as displayed in the OpenMC console window during runtime simulation. It was observed that after 8 batches the k values started to stabilize and thus the decision was made to skip 10 cycles. All simulations had less than 1 % relative error. The relative error of the cycle mean is $\frac{\sigma}{\mu}$, where σ is the standard deviation of the cycle mean and μ is the mean. Thus, less than 1 % relative error means relative errors are accurate to $1e-4$. The fuel in the core has been distributed in 6 rings; the number of fuel rods in each ring is listed in Table 3. Extensive eigenvalue runs were carried out by varying the enrichment value from 50 % to 70 % in each fuel ring to identify the sensitivity of each fuel ring.

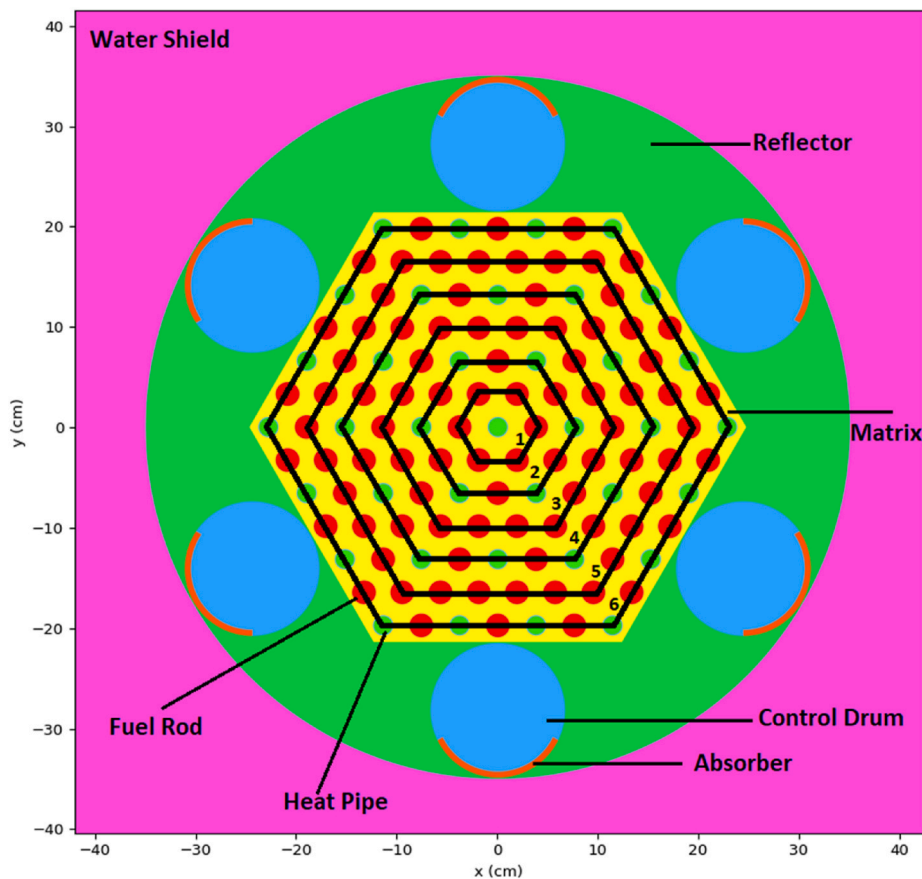


Fig. 1. Top view of the core. Shows the top view of the micro nuclear reactor core.

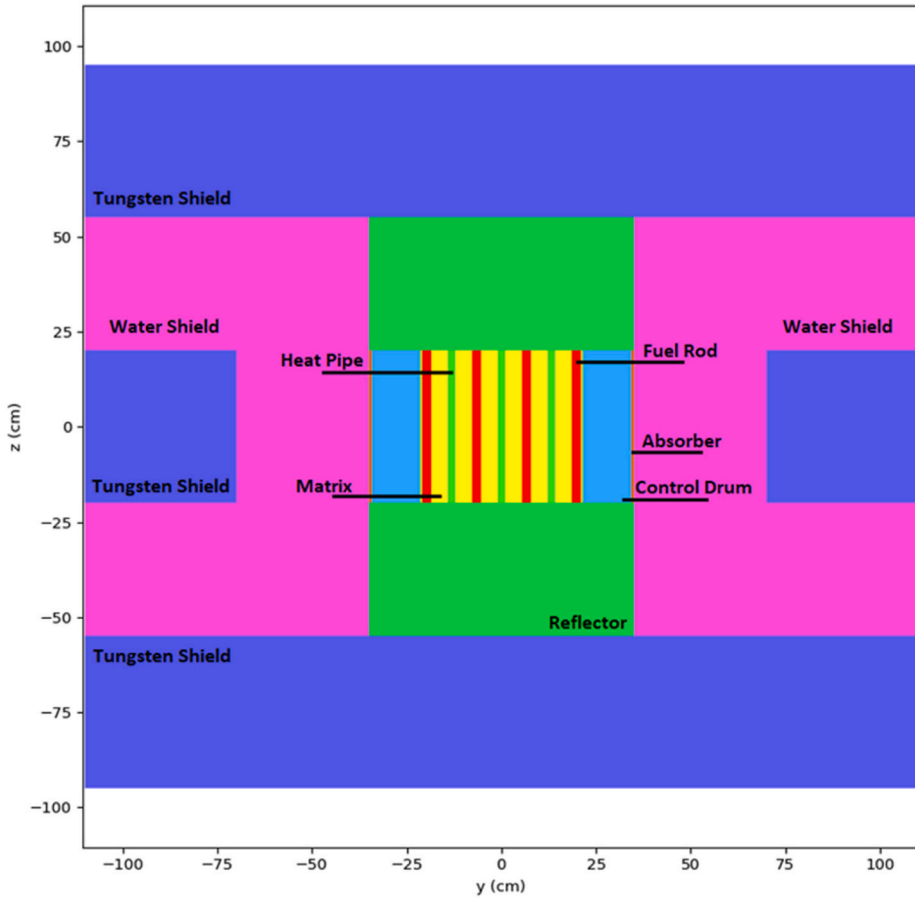


Fig. 2. Side view of the core. Shows the side view of the micro nuclear reactor core.

Table 1
MNHPR overall core design [1,2].

Parameter	Material
Fuel (enrichment)	UN (70 %)
Heat Pipe Working Fluid	Na (wick Mo-12Re)
Reflector/configuration	BeO/side and top
Control System	Control drums in reflector
Radiation Shield/configuration	Water and tungsten/side, top, and bottom

2.2. Thermomechanical performance

2.2.1. Heat transfer

Study of the heat transfer and temperature of fuel and cladding is an important part of the performance analysis. For smooth reactor operation, it is important to ensure that the operating temperature of the system does not exceed the safety limit i.e., the melting point. High temperature required for the megawatt thermal power results in thermal stress and consequently fuel swelling and release of fission gases occurs. Eq. (1) describes the heat transfer process in fuel and cladding. In the case of steady state, the differential term on left hand side of Eq. (1) becomes zero.

$$\frac{\partial(\rho c_p T)}{\partial t} = \frac{1}{r} \frac{\partial}{\partial r} \left(k.r \frac{\partial T}{\partial r} \right) + Q_0(r, t) \tag{1}$$

The thermal performance analysis has been carried out using COMSOL Multiphysics. Design parameters and correlations used to describe the materials in COMSOL are listed in Table 4.

Table 2
Core design parameters [1,2].

Design Parameter	Data
Fuel Rod	
Diameter (cm)	2.37
Height (cm)	40
Den (g cm ⁻³)	13.6
Cross-section area of fuel rod (cm ²)	4.4115
Mass fuel rod (kg)	2.3999
Temperature (K)	1200
Fuel-Clad Gap	
Thickness (μm)	100
Gas	Helium
Gap conductance ($\frac{W}{m^2.K}$)	2e4
Temperature (K)	1200
Fuel and Fissile Material	
No. of fuel rods	90
Area of fuel rods (cm ²)	397.0350
Mass of fuel rods (kg)/Mass of fuel rods/length (kg/cm)	215.99/5.3997
Heat Pipe	
No. of heat pipes	37
Working Fluid	Sodium
Radii Vapor/Wick/Liquid/Structure (cm)	0.90/0.92/1.00/1.02
Area of Heat Pipe (cm ²)	3.2685
Total area of heat pipes (cm ²)	120.9345
Den of vapor (g cm ⁻³)	0.01
Den of wick, structure (g cm ⁻³)	12.0, 12.0
Mass (kg), Mass/length (kg/cm)	12.8538/0.321345
Working Fluid Temperature (K)	1000
Matrix	
Material, Density (g cm ⁻³)	Nb-1Zr, 6.55
Area of Hexagon (cm ²)	1585.1
Area (Hexagon-Fuel-HP) (cm ²)	1067.1
Mass (kg), Mass/length (kg/cm)	279.58/6.9895
Temperature (K)	1100
Core	
Mass (kg)	508.424
Mass/length (kg/cm)	12.711
Axial Shield	
Top and Bottom shield water	35 cm
Top and Bottom shield tungsten	40 cm

Table 3
Fuel rods in each ring.

Fuel Ring	No. of Fuel Rods
1	6
2	6
3	18
4	12
5	30
6	18

2.2.2. Solid mechanics

During high temperature operation, the fuel and cladding undergoes thermal stress. If exposed to high temperature for longer duration the thermal stress may result in structural deformation. The radial (σ_r), hoop (σ_θ), and axial stresses (σ_z) in a long cylinder are given by Boley and Weiner [22] and are reproduced in Eq. (2a), Eq. (2b), and Eq. (2c):

$$\sigma_r = \frac{E\alpha}{1-\nu} \left[\frac{1}{R^2} \int_0^R T r dr - \frac{1}{r^2} \int_0^r T r dr \right] \tag{2a}$$

$$\sigma_\theta = \frac{E\alpha}{1-\nu} \left[\frac{1}{R^2} \int_0^R T r dr + \frac{1}{r^2} \int_0^r T r dr - T \right] \tag{2b}$$

$$\sigma_z = \frac{E\alpha}{1-\nu} \left[\frac{2}{R^2} \int_0^R T r dr - T \right] \tag{2c}$$

Table 4
Design parameters and correlations for materials in COMSOL.

Property	Correlation/Value	Units
Fuel (UN)		
Thermal conductivity (k_f)	$(1.37 \times T^{0.41}) \times \left(\frac{1-P}{1+P}\right)$ [16]	$\frac{W}{m \cdot K}$
Fuel porosity (P)	5	%
Coefficient of thermal expansion (α)	$(7.096 \times 10^{-6}) + (1.409 \times 10^{-9}) \times T$ [16]	$\frac{1}{K}$
Heat capacity (C_p)	$3.9683 \times \left(51.14 \times \left(\frac{365.7}{T}\right)^2 \times \frac{\exp\left(\frac{365.7}{T}\right)}{\left(\exp\left(\frac{365.7}{T}\right) - 1\right)^2} + 9.491 \times 10^{-3} \times T + 2.642 \times 10^{11} \times \left(\frac{1}{T^2}\right) \times \exp\left(-\frac{18081}{T}\right) \right)$ [20]	$\frac{J}{kg \cdot K}$
Density (ρ)	13,600	$\frac{kg}{m^3}$
Young's modulus (E)	$((0.258 \times D^{3.002}) \times (1 - 2.375 \times 10^{-5} \times T))$ [16]	Pa
Poisson's ratio (ν)	$(1.26 \times 10^{-3}) \times D^{1.174}$ [16]	-
Actual fuel density (D)	95	%TD
Cladding and Heat Pipe Wall (Mo-Re)		
Coefficient of thermal expansion (α)	4.8×10^{-6}	$\frac{1}{K}$
Density (ρ)	10,200	$\frac{kg}{m^3}$
Heat capacity (C_p)	250	$\frac{J}{kg \cdot K}$
Thermal conductivity (k_x)	138	$\frac{W}{m \cdot K}$
Young's modulus (E)	3.12×10^{11}	Pa
Poisson's ratio (ν)	0.31	-
Matrix (Nb-Zr)		
Coefficient of thermal expansion (α)	$(6.62 + (3.64 \times 10^{-4}) \times T + (2.75 \times 10^{-7}) \times (T^2)) \times 10^{-6}$ [21]	$\frac{1}{K}$
Density (ρ)	$8637 - 0.200 \times T$ [21]	$\frac{kg}{m^3}$
Heat capacity (C_p)	$\left(0.2441 + (5.105 \times 10^{-5}) \times T + \left(\frac{2.784 \times 10^9}{T^2}\right) \times \exp\left(-\frac{(2.295 \times 10^4)}{T}\right) \right) \times 10^3$ [21]	$\frac{J}{kg \cdot K}$
Thermal conductivity (k_m)	53	$\frac{W}{m \cdot K}$
Young's modulus (E)	104.9×10^9	Pa
Poisson's ratio (ν)	0.397	-

The generalized Hooke's law then gives the total strains as Eq. (3a), Eq. (3b), and Eq. (3c) [23].

$$\epsilon_r = \frac{1}{E} [\sigma_r - \nu(\sigma_\theta + \sigma_z)] + \alpha(T - T_o) + \epsilon^s + \epsilon^c \tag{3a}$$

$$\epsilon_\theta = \frac{1}{E} [\sigma_\theta - \nu(\sigma_r + \sigma_z)] + \alpha(T - T_o) + \epsilon^s + \epsilon_\theta^c \tag{3b}$$

$$\epsilon_z = \frac{1}{E} [\sigma_z - \nu(\sigma_r + \sigma_\theta)] + \alpha(T - T_o) + \epsilon^s + \epsilon_z^c \tag{3c}$$

The thermal creep for UN fuel is given by Eq. (4) [24].

$$\dot{\epsilon} = 2.054 \times 10^{-3} \sigma^{4.5} e^{-\frac{39369.5}{T}} \left(\frac{0.987 e^{-8.65Por}}{(1-P)^{27.6}} \right) \tag{4}$$

The analysis of mechanical behavior has been carried out using COMSOL Multiphysics and following assumptions has been considered while modeling the behavior in COMSOL:

1. Fuel has been assumed to be a continuous single entity, i.e., fuel pellets always remain in close contact with each other without any gaps.
2. Quasistatic structural transient behavior has been considered.
3. The solid model is isotropic.

3. Results and discussion

3.1. Thermomechanical analysis of fuel

For thermomechanical analysis, the system from fuel rod to heat pipe casing has been modeled as concentric cylinders. Fuel has been modeled with 95 % theoretical density to accommodate fission gases and swelling. Temperature dependence of material properties has been considered. It is desired to maintain a stable temperature at the heat pipe surface; a lower temperature will affect the performance of the sodium heat pipe, and a too high temperature will lead to wick dry out. For megawatt thermal power, each fuel rod will have steady state operating condition of ~11.11 kW. By volume equivalent method the single cell units have been considered as a cylindrical channel. Fig. 3 shows the equivalent control volume and Table 5 lists the radii of the units of the equivalent control volume. The reactor core’s complex geometry has been represented by representative cylindrical volumes or cells. Each cell is designed in such a way that it accurately reflects the volume and thermal characteristics of the complex geometry. This allows for a simpler geometry for analysis while retaining properties of the complex geometry. The equivalent control volume shown in Fig. 3 thus represents a single unit within the complex reactor core from center of a fuel rod to the wall of the adjacent heat pipe (fuel-gap-cladding-matrix-heat pipe wall).

Using the thermal resistance network model technique, the fuel centerline temperature has been calculated to analyze whether the fuel temperature remains within safety limits. It is desired to ensure that the temperature at the heat pipe wall remains within the operating limit of the working fluid. Fig. 4 shows the thermal resistance network model for the equivalent control volume.

In the network shown in Fig. 4, R1–R5 represent the fuel, gap, cladding, matrix, and heat pipe wall resistances, respectively. With the known desired temperature at the heat pipe wall the maximum center line temperature (T_{fc}) can be calculated using Eq. (5).

$$q = \frac{(T_{fc} - T_{hpw})}{R1 + R2 + R3 + R4 + R5} \tag{5}$$

For a sodium heat pipe, the operating temperature range is 900 K-1100 K [25]. In this analysis, the heat pipe wall temperature has been kept at 1000 K to ensure that the heat pipe operates efficiently without facing issues such as dry wick. Maintaining 1000 K also ensures a stable heat supply at heat pipe evaporator, minimizing the fluctuations that might arise due to slight change in the fuel temperature. Thus, ensuring reliable, and stable heat pipe performance. For 1000 K temperature at the heat pipe wall, a fuel center line temperature of 1246 K is calculated which is well within the safety limits of the UN fuel.

3.1.1. Temperature profile

Simulations have been carried out using COMSOL Multiphysics to study the temperature profiles. Fig. 5 shows the radial temperature from center of the fuel to heat pipe wall. The temperature 976 K is maintained at the heat pipe wall; the fuel center temperature reaches 1192 K for megawatt thermal power operation and is within the safety limits. There is a sharp temperature drop of 92 K in the fuel-clad gap. Due to the sharp temperature drop, the gap between the fuel and clad cannot be left arbitrarily large as it can severely impact the performance of the system.

Additionally, it can also be seen from Fig. 5 that the monolith, made of Nb-1Zr, is at ~20 K higher temperature than the heat pipe wall. Nb-1Zr is a refractory material with a high melting temperature of ~2700 K [26] and is known for high temperature applications that can withstand high thermal stresses [27]. Thus, the monolith is also well within its safe temperature limit for structural integrity.

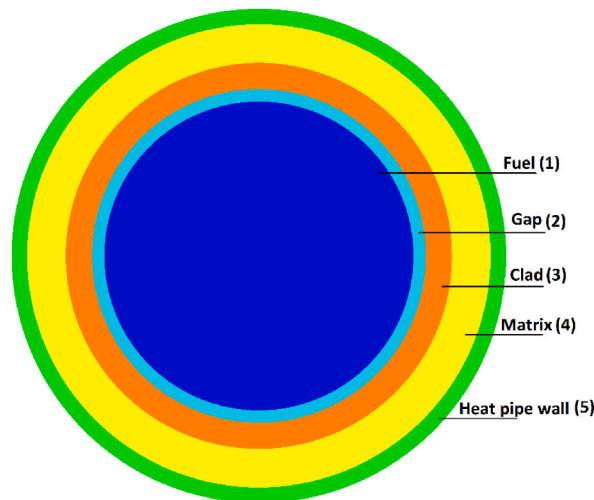


Fig. 3. Equivalent control volume.

Shows the equivalent control volume of the core that is used to create the thermal resistor network mode, starting from center of the fuel rod to the wall of the heat pipe.

Table 5
Percentage change in k_{eff} for 70 %–50 % enrichment change.

Parameter	Cell	Radius (cm)	Thermal Resistance
Radius 1 (r_f)	Fuell	1.185	$R1 = \frac{r_f}{k_f}$
Radius 2 (r_g)	Gap	1.195	$R2 = 1/h_g$
Radius 3 (r_c)	Cladding	1.219	$R3 = \frac{r_c - r_g}{k_c}$
Radius 4 (r_m)	Matrix	1.5898	$R4 = \frac{r_m - r_c}{k_m}$
Radius 5 (r_{hpw})	Heat Pipe Wall	1.6098	$R5 = \frac{r_{hpw} - r_m}{k_{hpw}}$
Length (l)	Length of all cylinders	40	–

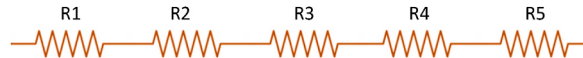


Fig. 4. Thermal resistance network model.
Shows the thermal resistor network model of the core starting from center of the fuel rod to the wall of the heat pipe.

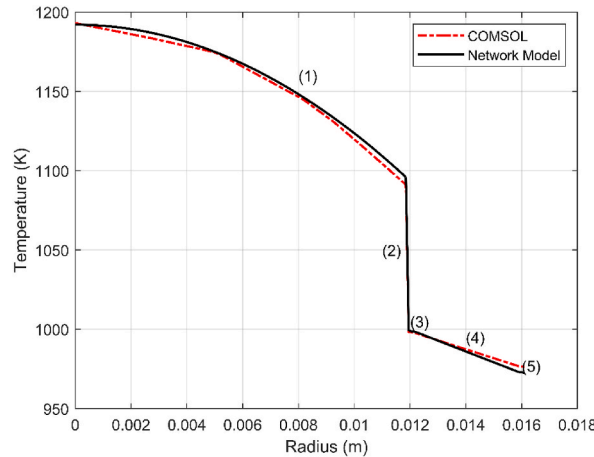


Fig. 5. Radial temperature.
Shows the radial temperature profile from center of the fuel to the heat pipe wall.

Results from COMSOL were verified using thermal resistance network model. Results from network model and COMSOL agree, and a maximum difference of 4 K is observed at fuel surface and a difference of 3 K is observed at heat pipe wall. For megawatt operation the fuel temperature remains well within the safety limit of 2000K and there is apparent room to increase thermal power.

3.1.2. Solid mechanics

During high temperature operation the system undergoes thermal stresses resulting in strain and deformation. Displacement can provide an intuitive insight into the mechanical state of the fuel [16]. Fig. 6 shows the displacement of fuel for three power levels, i.e., 1 MW_{th}, 1.1 MW_{th}, and 1.5 MW_{th}. The full core thermal power is divided between 90 fuel rods. Maximum radial displacement of 97.4 μm is observed in the fuel for long term operation at megawatt thermal power (11.11 kW per fuel rod); the displacement is within the 100 μm fuel-clad gap in the design.

To check the reactor performance beyond 1MW_{th} more analyses were carried out. For 1.1MW_{th}, i.e., an increase of 100kW_{th}, the radial displacement of 107.2 μm is observed with fuel center temperature reaching 1250 K. For 1.5MW_{th}, the fuel centerline temperature reaches 1534 K and radial displacement is 143.8 μm. Although the fuel temperature remains well within the 2000K limit, the radial displacement, which represents the swelling of the fuel, does not allow further increase in thermal power.

If the power is evenly distributed in the core, the system can sustain megawatt thermal power operation while remaining within safety parameters. Thus, an analysis of power distribution in the core has been carried out.

3.2. Radial power peaking

Power distribution has been estimated by tallying the fission reaction rate using OpenMC Monte Carlo particle transport code, and

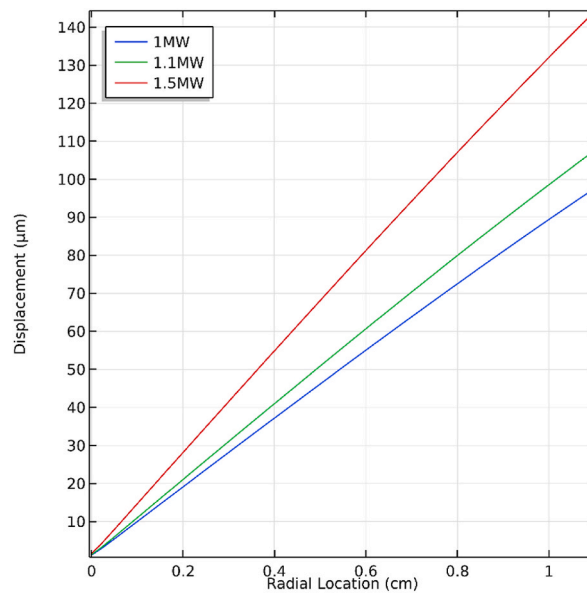


Fig. 6. Radial displacement. Shows the displacement of fuel for three power levels, i.e., 1 MWth, 1.1 MWth, and 1.5 MWth.

1/6th symmetry in the core has been observed. Thus, the results related to power peaking and its mitigation are presented for 1/6th of the core. The effective multiplication factor, k_{eff} , for 70 % enriched uniformly distributed fuel is estimated as 1.00080 with a relative error of ± 0.00091 .

With the uniform distribution of fuel i.e., 70 % enriched fuel in all rings, an uneven power distribution is observed, and the core undergoes as much as 22 % radial power peaking as shown in Fig. 7a. The average fuel centerline temperature is 1192.

The analysis of power distribution in the core shows that there are different power levels inside the core. These different power levels result in different fuel temperatures and consequently different thermal stress. The fuel centerline temperature and subsequent displacement in each fuel rod is shown in Fig. 7b and c, respectively. Orange and yellow color grids represent the cases where the parameter value is higher than the desired value. Green grids represent that the value is within desired and acceptable parameters, whereas blue grid indicates that the parameter value is less than the desired value.

The maximum temperature of 1353 K in the innermost fuel ring is within the safety margin, however, the displacement or swelling, for all cases where peaking factor is greater than 1, exceeds the design limitation. Because of power peaking, the reactor must be operated at least 22 % less than the desired power levels for it to remain within safety parameters.

3.3. Fuel ring sensitivity to enrichment

Monte Carlo simulations were carried out by varying the enrichment of UN fuel in each ring from 50 % to 70 %. Enrichment was changed by 1 % in each fuel ring at a time, while the remaining fuel rings were kept at 70 %. In the Beginning of Life (BOL) as shown in Fig. 8, for MNR, the value of $k_{eff} > 1$, the control drums will face towards the core to adjust the excess reactivity and maintain $k_{eff} = 1$. After the reactor starts its operation, the reactivity decreases, and k_{eff} falls below 1 due to fuel burnup. To accommodate the decrease in reactivity, the control drums begin to move away from the core. When the control drums face entirely away from the core, it will be the reactor's End of Life (EOL).

Fig. 8 shows the change in k_{eff} with change in enrichment in each fuel ring when the control drums are facing away from the core. Fig. 9 shows the relative slope of change in k_{eff} for each fuel ring compared to the innermost ring, i.e., ring 1. The relative slope, which represents the sensitivity of each fuel ring, has been calculated using the method of curve fitting. MATLAB has been used to fit a polynomial to the 3rd order using the *polyfit* command. Slopes of the polynomials were then compared, and the relative slope was obtained using MATLAB.

Fig. 8 shows that rings 5 and 3 are two of the most sensitive rings, respectively, as they result in the highest decrease in the value of k_{eff} when enrichment is reduced, whereas ring 2 is the least sensitive fuel ring, followed by ring 1. The higher sensitivity of rings 5 and 3 is also evident from their higher relative slope. Ring 5 has a 3.3 times higher relative slope, and ring 3 has 2.7 times higher relative slope, relative to ring 1. The higher relative slope and sensitivity to the enrichment of these rings can be attributed to the fact that these rings contain the highest and second-highest number of fuel rods, respectively, and that these rings do not contain any heat pipe whereas the even-numbered rings, 2, 4, and 6 consists of fuel rods and heat pipes. Table 6 lists the percentage change in k_{eff} when enrichment is changed from 70 % to 50 % for each fuel ring as well as results normalized to per fuel rod. The sensitivity per rod in rings 4, 5, and 6 is found to be lower than for other rings; however, the cumulative reactivity is higher.

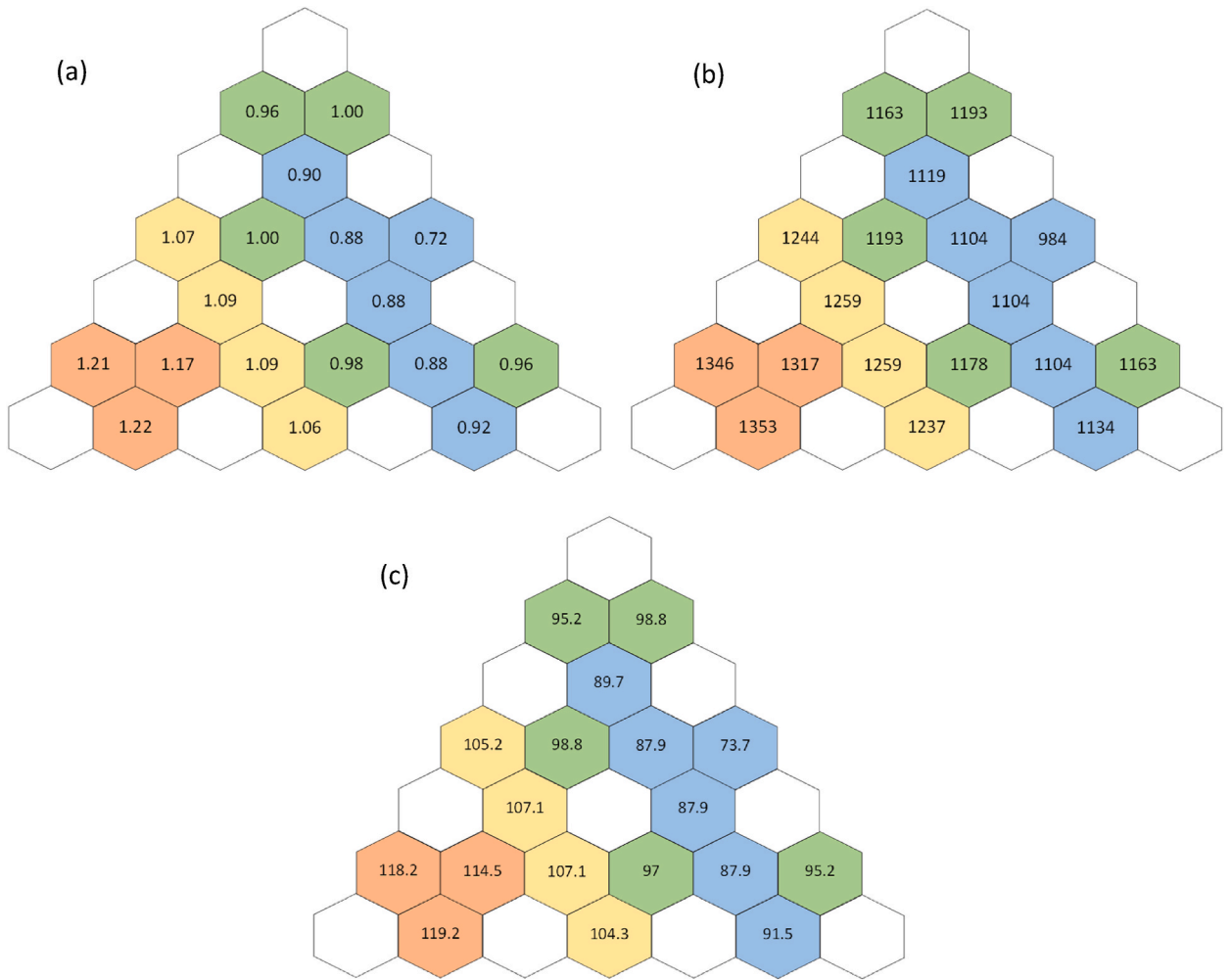


Fig. 7. Uniform fuel distribution (a) Radial power peaking (b) Temperature of each fuel ring in K (c) Displacement Magnitude in μm . a, b, and c shows the radial power peaking factor, maximum temperature of each fuel ring in Kelvin, and displacement magnitude in microns, respectively, when the fuel enrichment is kept same in the core.

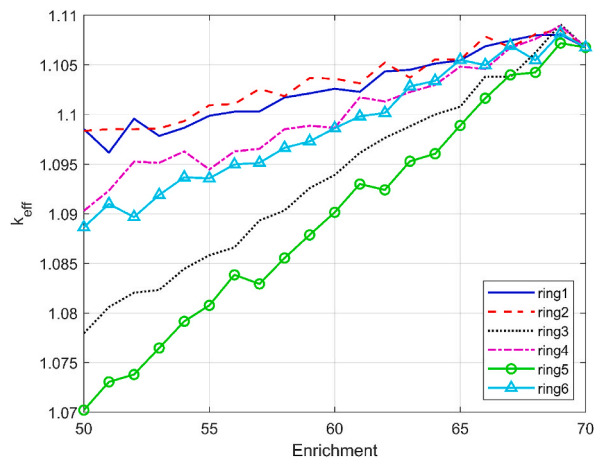


Fig. 8. Change in reactivity with change in enrichment for BOL (control drums facing away from the core). Shows the effect of changing the enrichment in each fuel ring on k_{eff} .

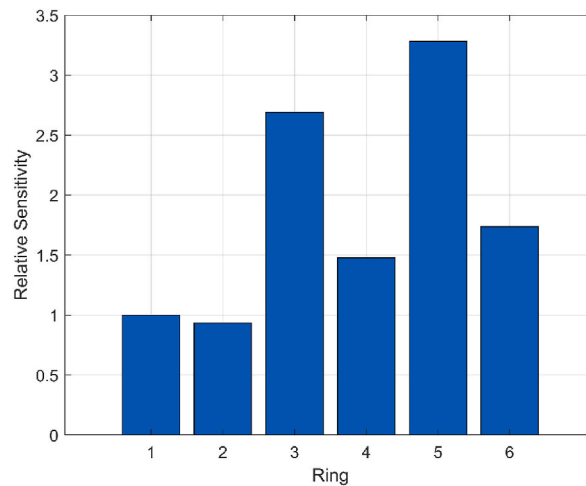


Fig. 9. Relative sensitivity of fuel rings. Shows the relative sensitivity of fuel rings to change in enrichment.

Table 6
Percentage change in k_{eff} for 70 %–50 % enrichment change.

Ring	Percent Change in each Ring	Percent Change in each Ring Normalized to per fuel Rod
1	0.7492	0.1249
2	0.7657	0.1276
3	2.6727	0.1485
4	1.5097	0.1258
5	3.4152	0.1138
6	1.6645	0.0925

The sensitivity analysis shows the presence of distinct power zones within the core. The presence of distinct power zones is attributed to varying fuel burn up. These findings regarding power distribution are consistent with the findings of Goldschmidt and Quenon [28]. György and Czifrus [29] have also reported similar power distribution trends in a low-enriched plutonium reactor.

Fuel rings of the hexagonal core can thus be divided into three zones, i.e., the inner zone, the middle zone, and the outer zone. Inner and outer zones consist of rings 1, and 6 respectively, whereas rings 2–5 form the middle zone. The innermost rings undergo the highest burnup and thus result in power peaking in the inner zone. Similarly, the outermost ring undergoes higher burnup because of its proximity to the reflector and reflected neutrons. Power peaking in the outermost zone is more prominent at EOL when the control drums (absorber) are facing away from the core.

3.4. Power peaking mitigation

Based on the sensitivity analysis the use of variable enrichment i.e., non-uniform distribution of fuel in the core is proposed. To verify its effectiveness two cases have been considered; i) divide the core into three zones, ii) treat each fuel ring as a separate zone.

3.4.1. Case 1

For this case, the core has been divided into three zones: inner-, middle-, and outer-zones and the fuel of different enrichment was placed in the inner and outer zone. Inner and outer zones consist of rings 1, and 6 respectively, whereas rings 2–5 form the middle zone. For this case, min-max-min fuel distribution strategy is adopted.

When the variable enriched fuel is used, 70 % in the middle zone and 67 % in the inner and 64 % outer zones respectively, the multiplication factor is estimated as 1.00027 with relative error ± 0.00086 . Fig. 10a shows the power peaking with non-uniform distribution of fuel in the core. Fig. 10b and c show the resulting fuel centerline temperature and swelling of each fuel rod, respectively.

The use of min-max-min fuel distribution strategy has improved the overall peaking in the core with the average fuel temperature 1192 K. The reduction of overall peaking factor, albeit small, has improved the maximum operating power of reactor by $\sim 5\%$ to 811 kW for desired megawatt operation. The peaking factor of 1.19 in the ring 2 still significantly hinders the improvement in the core performance.

3.4.2. Case 2

In case 2 each fuel ring has been considered as an independent zone. The non-uniform distribution of the fuel follows the gradual increase of enrichment from ring 1 to ring 5 with max enrichment in ring 5, and then a drop in the enrichment to mitigate any peaking

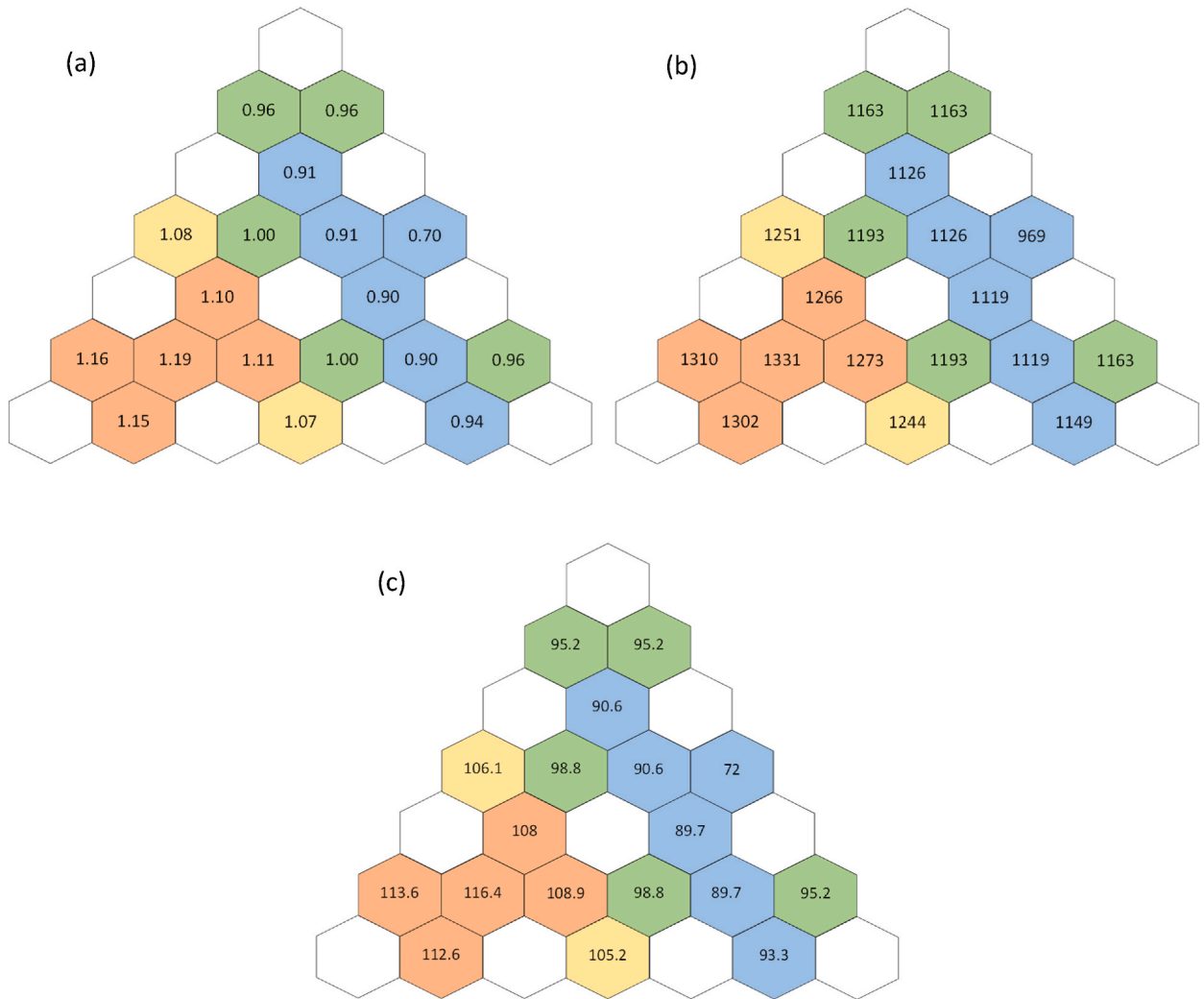


Fig. 10. Non-uniform fuel distribution case 1 (a) Case1: Radial power peaking (b) Case1: Temperature of each fuel ring in K (c) Case1: Displacement Magnitude in μm .

a, b, and c shows the radial power peaking factor, maximum temperature of each fuel ring in Kelvin, and displacement magnitude in microns, respectively, when the fuel rings are divided into 3 enrichment zones.

in ring 6 due to its proximity to the reflectors.

From ring 1 to ring 6 fuel of 60-62-70-70-75-65 percent enrichment has been placed. The multiplication factor is estimated as 1.00016 with relative error ± 0.00097 . Fig. 11a shows the peaking factor, Fig. 11b shows the fuel centerline temperature, and Fig. 11c shows the swelling in each fuel rod for case 2.

A significant improvement in the overall peaking has been observed. The maximum peaking factor of 1.11 is observed in ring 3. The average fuel centerline temperature of the core has increased by 3 K–1195 K. With the improvement in power peaking, the maximum operating power is also increased by 15 % to 893 kW for the desired megawatt power level.

The analysis thus far has been carried out to establish the maximum allowable limit for normal reactor operation which corresponds to 1 Factor of Safety (FoS). With 1.5 FoS the maximum safe operating power is 579 kW for uniform distribution and 667 kW for case 2 of non-uniform distribution; with 2 FoS the limits are 349 kW and 402 kW for uniform and case 2 non-uniform distribution, respectively.

The use of non-uniform fuel distribution is thus a viable peaking mitigation technique that can significantly enhance the performance of the MNR without any physical design change. Comparison of various parameters for using uniform and non-uniform fuel distribution in the core is presented in Table 7.

4. Conclusions

A Micro Nuclear Heat Pipe Reactor (MNHPR) with Highly Enriched Uranium (HEU) fuel is modeled and simulated with the Monte

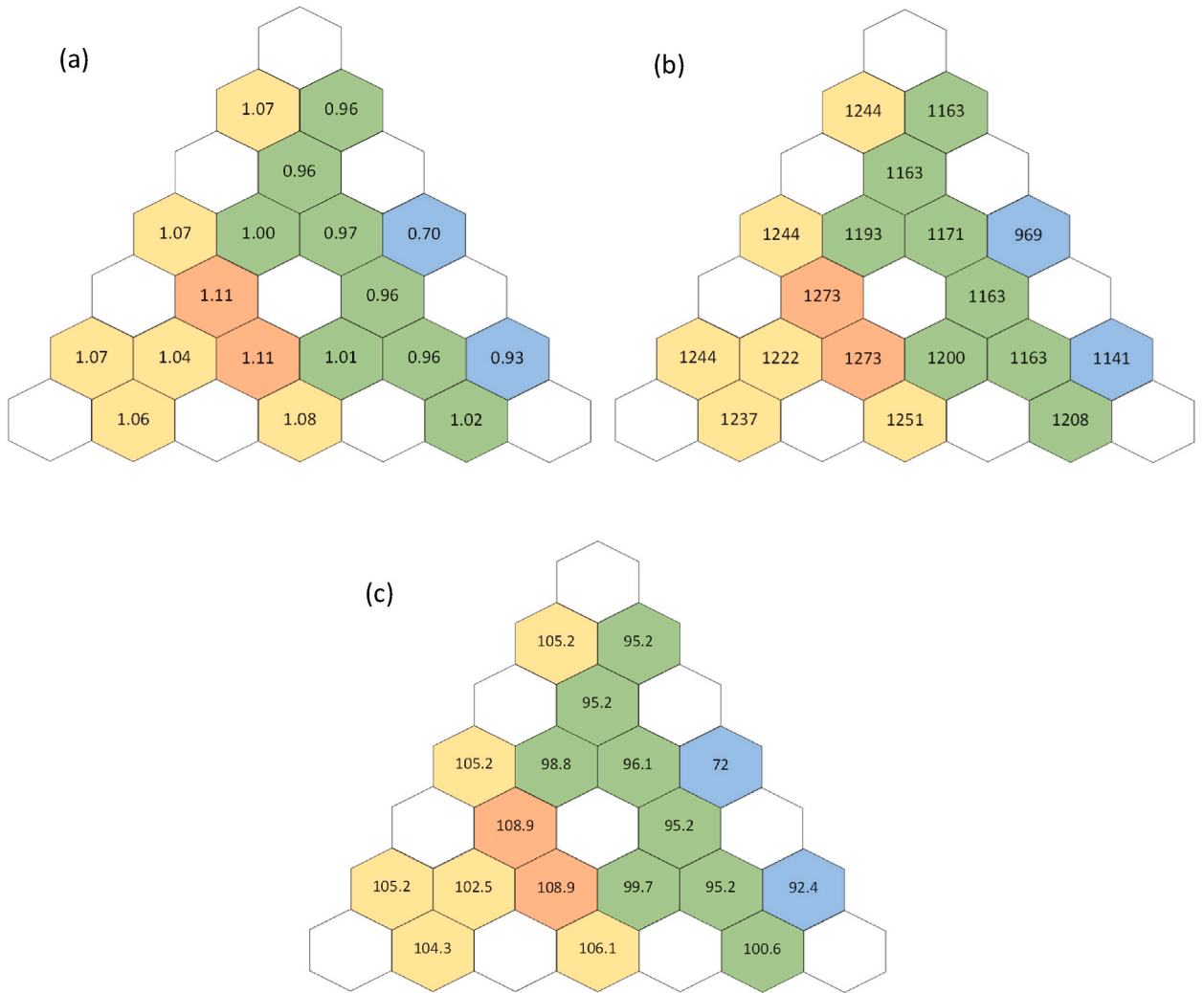


Fig. 11. Non-uniform fuel distribution case 2 (a) Case2: Radial power peaking (b) Case2: Temperature of each fuel ring in K (c) Case2: Displacement Magnitude in μm .
 a, b, and c shows the radial power peaking factor, maximum temperature of each fuel ring in Kelvin, and displacement magnitude in microns, respectively, when each fuel ring is considered as a separate zone.

Table 7
 Comparison of uniform and non-uniform fuel distribution.

Parameter	Uniform Distribution	Non-uniform Distribution Case 1	Non-uniform Distribution Case 2
Enrichment in each ring	70 %	65-70-70-70-65	60-62-70-70-75-65
Max Peaking Factor	1.22	1.19	1.11
Max Fuel Centerline Temp	1353 K	1331 K	1273 K
Avg Fuel Centerline Temp	1191 K	1192 K	1195 K
Max power (FoS = 1.0)	775 kW	811 kW	893 kW
Max power (FoS = 1.5)	579 kW	606 kW	667 kW
Max power (FoS = 2.0)	349 kW	365 kW	402 kW
Enhancement in power	–	~5 %	15 %

Carlo code OpenMC. The heat pipes use sodium as the working fluid at ~ 1000 K for megawatt thermal operation. Overall, the MNHPR is feasible as a power source for specialized applications, space exploration missions, and off-grid installations. The total uranium fuel is ~ 216 kg which constitutes about one-fourth of the compact cylindrical (radius 35 cm, height 40 cm) core mass. HEU-fueled Micro Nuclear Reactors (MNR), like thermal power plants, also suffer from Radial Power Peaking (RPP) which significantly reduces the maximum allowable operating thermal power. In this design, radial peaks have been observed in the various regions of the hexagonal

core. The use of non-uniform fuel distribution is found to be one viable solution to mitigate the power peaking. A higher initial excess reactivity could also be explored to prolong the reactor life; to compensate for such an excess reactivity, it is suggested to consider coatings of burnable absorbers on fuel rods for initial reactor operation. Extensive Monte Carlo simulations have been carried out to understand which regions of the core are more sensitive to enrichment (ϵ) changes (change in k_{eff} with change in enrichment, $\delta k_{eff} / \delta \epsilon$). The use of non-uniform fuel distribution (variable enrichment) in the core results in an acceptable reduction in the power peaking. Using the non-uniform fuel placement strategy proposed in this work, 15 % enhancement in the maximum allowable operating power can be achieved without any design change. This work has considered the radial power peaking in the core. A study was not carried out on axial peaking. The complete mitigation of the peaking, however, requires optimization study while considering axial power peaking as well for an optimal non-uniform distribution. Therefore, further work is recommended in extending this work to axial distributions, which will affect the heat transport through the heat pipes. A reduction in the RPP, however, does reduce thermal-induced stresses in the core, increasing its resilience in the event of any excursion.

Data availability statement

All data used in this manuscript have been presented within the article.

CRediT authorship contribution statement

Umair Aziz: Writing – original draft, Validation, Software, Methodology, Investigation, Formal analysis, Data curation, Conceptualization. **Zafar U. Koreshi:** Writing – review & editing, Supervision, Conceptualization. **Hamda Khan:** Methodology, Investigation, Formal analysis, Data curation. **Shakil R. Sheikh:** Writing – review & editing, Supervision, Conceptualization.

Declaration of competing Interest

The authors declare that they have no known competing financial interests or personal relationships that could have appeared to influence the work reported in this paper.

Nomenclature

B_4C	Boron Carbide
BOL	Beginning of Life
l	Core length
Q	Creep activation energy $\left[327160 \frac{J}{mol} = 78.2 \frac{kcal}{mol} \right]$
k_{eff}	Effective multiplication factor
EOL	End of Life
r_m	Equivalent unit cell radius of core matrix
r_{hpw}	Equivalent unit cell radius for heat pipe wall
FoS	Factor of Safety
T_{fc}	Fuel Center Temperature [K]
r_g	Fuel-clad gap radius
r_c	Fuel cladding radius
P	Fuel porosity
r_f	Fuel radius
h_g	Gap conductance $\left[\frac{W}{m^2 \cdot K} \right]$
q	Heat flux $\left[\frac{W}{m^2} \right]$
T_{hpw}	Heat Pipe Wall Temperature [K]
HEU	Highly Enriched Uranium
KRUSTY	Kilopower Reactor Using Stirling Technology
kW	kilowatt
kWe	Kilowatt electric
MNR	Micro Nuclear Reactors
MNHPR	Micro Nuclear Heat Pipe Reactors
MC	Monte Carlo
MW	Mega Watt
MWe	Megawatt Electric
MWth	Megawatt Thermal
PWR	Pressurized Water Reactors

r	Radial distance [cm]
RPP	Radial Power Peaking
c_p	Specific heat $\left[\frac{J}{kg \cdot K}\right]$
TEG	Thermo Electric Generator
t	Time [s]
T	Temperature [K]
k	Thermal conductivity $\left[\frac{W}{m \cdot K}\right]$
UO ₂	Uranium Dioxide
UN	Uranium Nitride
Q_0	Volumetric heat source $\left[\frac{W}{m^3}\right]$
E	Young's modulus [Pa]
α	Coefficient of thermal expansion $\left[\frac{1}{K}\right]$
ϵ	Enrichment
ϵ_r	Radial strain
ϵ_θ	Circumferential strain
ϵ_z	Axial strain
ϵ^s	fuel swelling strain
ϵ_r^c	Radial creep strain
ϵ_θ^c	Circumferential creep strain
ϵ_z^c	Axial creep strain
$\dot{\epsilon}$	Thermal creep
ρ	density $\left[\frac{kg}{m^3}\right]$
σ_r	Radial stress
σ_θ	Hoop stress
σ_z	Axial stress
μ	mean
ν	Poisson's ratio

References

- [1] H. Sun, C. wang, P. Ma, X. Liu, W. Tian, S. Qiu, G. Su, Conceptual design and analysis of a multipurpose micro nuclear reactor power source, *Ann. Nucl. Energy* 121 (2018) 118–127, <https://doi.org/10.1016/j.anucene.2018.07.025>.
- [2] U. Aziz, Z.U. Koreshi, S.R. Sheikh, H. Khan, A study of criticality and thermal loading in a conceptual micronuclear heat pipe reactor for space applications, *Nucl. Technol. Radiat. Protect.* 35 (2020) 208–215, <https://doi.org/10.2298/NTRP2003208A>.
- [3] A. Levinsky, J.J. Van Wyk, Y. Arafat, M.C. Smith, Westinghouse eVinci TM Reactor for Off-Grid Markets, in: *Trans Am Nucl Soc, Orlando, Florida, 2018*, pp. 931–934. <http://answinter.org/wp-content/2018/data/pdfs/404-26706.pdf>. (Accessed 25 January 2019).
- [4] D.I. Poston, M. Gibson, P. McClure, Kilopower reactors for potential space exploration missions, in: *Nuclear and Emerging Technologies for Space, American Nuclear Society Topical Meeting, ANS, Richland, WA, USA, 2019*.
- [5] D.I. Poston, P.R. McClure, D.D. Dixon, M.A. Gibson, L.S. Mason, Experimental demonstration of a heat pipe-Stirling engine nuclear reactor, *Nucl. Technol.* 188 (2014) 229–237, <https://doi.org/10.13182/NT13-71>.
- [6] K.J. Geelhood, D.V. Colameco, W.G. Luscher, L. Kyriazidis, C.E. Goodson, J. Corson, FAST-1.0.1: A Computer Code for Thermal-Mechanical Nuclear Fuel Analysis under Steady-State and Transients, 2021. <https://www.ntis.gov/about>.
- [7] X. Zhang, Z. Wang, Y. Xi, W. Liu, Y. Deng, D. Yun, 3-Dimensional Multiphysics modeling of behaviors of pressurized water reactor fuel rods with missing pellet surface, *Front. Energy Res.* 9 (2021) 738084, <https://doi.org/10.3389/fenrg.2021.738084>.
- [8] M.Y.M. Mohsen, M.S. Hassan, M. Aziz, M.A.E. Abdel-Rahman, Investigating the Neutronic, Thermal-Hydraulic, and Solid Mechanics Analysis for AP-1000 Nuclear Reactor, *Energy Sources, Part A: Recovery, Utilization, and Environmental Effects*, 2021, pp. 1–23, <https://doi.org/10.1080/15567036.2021.1912215>.
- [9] K.L. Murty, I. Charit, *An Introduction to Nuclear Materials: Fundamentals and Applications*, John Wiley & Sons, 2013.
- [10] J.P. Ellington, Temperatures, thermal stresses and displacements in solid uranium dioxide rods, *Br. J. Appl. Phys.* 11 (1960) 33, <https://doi.org/10.1088/0508-3443/11/1/305>.
- [11] R.F. Canon, J.T.A. Roberts, R.J. Beals, Deformation of UO₂ at high temperatures, *J. Am. Ceram. Soc.* 54 (1971) 105–112, <https://doi.org/10.1111/j.1151-2916.1971.tb12230.x>.
- [12] T. Tachibana, H. Furuya, M. Koizumi, Dependence on strain rate and temperature shown by yield stress of uranium dioxide, *J. Nucl. Sci. Technol.* 13 (1976) 497–502, <https://doi.org/10.1080/18811248.1976.9734063>.
- [13] S.L. Hayes, J.K. Thomas, K.L. Peddicord, Material property correlations for uranium mononitride: IV. Thermodynamic properties, *J. Nucl. Mater.* 171 (1990) 300–318, [https://doi.org/10.1016/0022-3115\(90\)90377-Y](https://doi.org/10.1016/0022-3115(90)90377-Y).
- [14] W. Li, K. Shirvan, Multiphysics phase-field modeling of quasi-static cracking in urania ceramic nuclear fuel, *Ceram. Int.* 47 (2021) 793–810, <https://doi.org/10.1016/j.ceramint.2020.08.191>.
- [15] H. Yuan, G. Wang, R. Yu, Y. Tao, Z. Wang, S. Guo, W. Liu, D. Yun, L. Gu, Lead-cooled fast reactor annular UN fuel design and development of performance analysis program, *Front. Energy Res.* 9 (2021) 705944, <https://doi.org/10.3389/fenrg.2021.705944>.

- [16] C. Wang, H. Sun, S. Tang, W. Tian, S. Qiu, G. Su, Thermal-hydraulic analysis of a new conceptual heat pipe cooled small nuclear reactor system, *Nucl. Eng. Technol.* 52 (2020) 19–26.
- [17] X. Liu, H. Sun, S. Tang, C. Wang, W. Tian, S. Qiu, G. Su, Thermal-hydraulic design features of a micronuclear reactor power source applied for multipurpose, *Int. J. Energy Res.* 43 (2019) 4170–4183, <https://doi.org/10.3389/tenrg.2021.705944>.
- [18] P.K. Romano, N.E. Horelik, B.R. Herman, A.G. Nelson, B. Forget, K. Smith, OpenMC: a state-of-the-art Monte Carlo code for research and development, *Ann. Nucl. Energy* 82 (2015) 90–97, <https://doi.org/10.1016/j.anucene.2014.07.048>.
- [19] COMSOL Multiphysics® v. 6.2. COMSOL AB, Stockholm, Sweden.
- [20] International Atomic Energy Agency., Thermophysical Properties of Materials for Nuclear Engineering : a Tutorial and Collection of Data., n.d..
- [21] D.J. Senior, J.K. Thomas, K.L. Peddicord, Thermophysical Property Correlations for the Niobium-1 % Zirconium Alloy, 1990, [https://doi.org/10.1016/0022-3115\(90\)90394-3](https://doi.org/10.1016/0022-3115(90)90394-3).
- [22] B.A. Boley, J.H. Weiner, *Theory of Thermal Stresses*, John Wiley & Sons, 1962.
- [23] S. Timoshenko, J. Goodier, *Theory of Elasticity*, McGraw-Hill Book Co., Inc., 1951.
- [24] S.L. Hayes, J.K. Thomas, K.L. Peddicord, Material Property Correlations for Uranium Mononitride II. Mechanical Properties, 1990, [https://doi.org/10.1016/0022-3115\(90\)90375-W](https://doi.org/10.1016/0022-3115(90)90375-W).
- [25] M. El-Genk, J.-M. Tournier, Uses of liquid-metal and water heat pipes in space reactor power systems, *Front. Heat Pipes (FHP)*. 2 (2011), <https://doi.org/10.5098/fhp.v2.1.3002>.
- [26] K.J. Leonard, J.T. Busby, S.J. Zinkle, Influence of thermal and radiation effects on microstructural and mechanical properties of Nb-1Zr, *J. Nucl. Mater.* (2011) 286–302, <https://doi.org/10.1016/j.jnucmat.2011.04.018>.
- [27] A.N. Behera, A. Chaudhuri, R. Kapoor, J.K. Chakravarty, S. Suwas, High temperature deformation behavior of Nb-1wt.%Zr alloy, *Mater. Des.* 92 (2016) 750–759, <https://doi.org/10.1016/j.matdes.2015.12.077>.
- [28] P. Goldschmidt, J. Quenon, Minimum critical mass in fast reactors with bounded power density, *Nucl. Sci. Eng.* 39 (1970) 311–319, <https://doi.org/10.13182/nse70-a19992>.
- [29] H. György, S. Czifrus, Burnup calculation of the Generation IV reactors, *Prog. Nucl. Energy* 81 (2015) 150–160, <https://doi.org/10.1016/j.pnucene.2015.01.015>.